

Article

# Effect of Tantalum Addition on Properties of Cu–Zr–Based Thin Film Metallic Glasses (TFMGs)

Sofiane Achache <sup>1,\*</sup> and Frederic Sanchette <sup>2,\*</sup> 

<sup>1</sup> ICD-LASMIS: Université de Technologie de Troyes, CNRS, Antenne de Nogent, Pôle Technologique de Sud Champagne, 26 Rue Lavoisier, 52800 Nogent, France

<sup>2</sup> Nogent International Center for CVD Innovation, LRC CEA-ICD-LASMIS, UTT, Antenne de Nogent-52, Pôle Technologique de Haute-Champagne, 52800 Nogent, France

\* Correspondence: sofiane.achache@utt.fr (S.A.); frederic.sanchette@utt.fr (F.S.); Tel.: +33-351-591-194 (S.A.); Fax: +33-3-25-71-76-76 (S.A.)

Received: 23 April 2020; Accepted: 25 May 2020; Published: 28 May 2020



**Abstract:** Cu–Zr–Ta ternary thin film metallic glasses (TFMGs) were deposited through the direct current (DC) magnetron sputtering of pure metallic targets in a dynamic mode. The effect of tantalum addition on the microstructure, mechanical properties, and thermal behavior of TFMGs were investigated. Nanoindentation measurements showed that an increase in tantalum content from 0 to 47 at % favored hardness and Young’s modulus, which rose from 5.8 to 11.23 Gpa and from 90 to 136 Gpa, respectively. XRD analysis and differential scanning calorimetry (DSC) measurements highlighted an improvement of thermal stability with the tantalum addition from 377 to 582 °C when the tantalum content increased from 0 to 31 at %.

**Keywords:** magnetron sputtering; mechanical properties; thermal stability; Cu–Zr–Ta alloys

## 1. Introduction

Bulk metallic glasses (BMGs) have attracted considerable attention due to their exceptional properties, which originate from their disordered atomic structure without grain boundaries. These properties are mainly high strength, superior elasticity and hardness, high corrosion resistance, and biocompatibility [1–6].

Thin film metallic glasses (TFMGs) with immiscible early transition metal–late transition metal mixtures, especially that of Cu–Zr, have already been widely studied [7–17]. These studies have shown that adding an appropriate amount of an alloying element leads to the enhancement of TFMG properties. For example, Zitek et al. investigated the effect of the addition of Al and Si into a Zr–Hf–Cu thin film that was deposited by magnetron sputtering [7]. They showed that adding Al up to 12 at % and Si up to 6 at % led to an increase of the crystallization temperature and to better mechanical properties. It has also been reported that adding higher amounts of these elements can lead to rapid crystallization. A similar effect of silicon was observed for Cu–Zr–Al and Cu–Ti–Zr–Ni TFMGs [18,19].

TFMGs have also been sputter deposited for micro-electromechanical systems (MEMS) and biomedical applications [20–22]. Zong et al. showed that TFMGs could be good candidates as transparent conducting oxide (TCO) electrodes for various applications [23]. Bouala and al. also showed that a Zr<sub>73</sub>Cu<sub>16</sub>Ag<sub>11</sub> TFMG could be a potential candidate for surgery tools and hospital furniture [22].

As mentioned above, the most studied TFMGs in the literature are Cu–Zr binary films. These films have interesting mechanical properties. However, they have a poor thermal stability. Thus, the aim of our study was to improve the thermal stability and mechanical properties of these films.

Ta is usually used as a minor addition element in the enhancement of the properties of various TFMGs. For example, Chen et al. showed that a Ta addition to a ZrCuAl TFMG led to an enhancement of its mechanical properties [24]. Chou et al. also observed the same behavior for a ZrCuTi TFMG [25]. However, the effect of high Ta contents on the thermal stability of TFMGs has not yet been reported.

Tantalum has a high atomic mass and a large atomic radius of 0.1457 nm [26]; it also exhibits a very high melting point of about 3025 °C [27], which makes it a promising candidate to improve the thermal stability of metallic glasses [28].

Therefore, this study concerned the effect of tantalum addition on the mechanical properties and thermal stability of Cu-Zr(-Ta)-based thin film metallic glasses that were deposited by DC magnetron sputtering.

## 2. Experimental Details

### 2.1. Deposition

Cu-Zr(-Ta) TFMGs were deposited from copper, zirconium, and tantalum targets (99.99% purity, 200 mm in diameter, and 6 mm thick) at a floating temperature without bias in pure argon (working pressure: 0.4 Pa; 30 sccm Ar). The target–substrate distance was constant at 10 cm, and deposition was carried out in a dynamic mode; the rotational speed of the substrate holder was fixed at 10 rpm in order to ensure the composition homogeneity of the films during growth. The deposition time was two hours, thus leading to films with thickness of about 2 µm.

Glass substrates were used for XRD and nanoindentation tests, and molybdenum sheets were used for DSC tests. Before deposition, all substrates were cleaned ultrasonically in acetone for 15 min, rinsed in ethanol and then dried with hot air. The chamber was pumped down to a pressure limit of  $9 \times 10^{-5}$  Pa, and then the substrates were sputter-cleaned before the deposition step at 200 W for 30 min using Ar<sup>+</sup> ions to remove undesirable oxides and contamination layers. The discharge currents were adjusted to keep the Cu at %/Zr at % ratio constant (Table 1; Section 3.1) and to allow for the control of the Ta content in the films.

**Table 1.** Discharge current and corresponding elemental compositions.

I <sub>cu</sub> (A)	I <sub>Zr</sub> (A)	I <sub>Ta</sub> (A)	Cu at %	Zr at %	Ta at %	Cu/Zr
0.2	1.4	0	36	64	0	0.56
0.6	1.2	0.2	30	52	18	0.57
0.6	1.2	0.4	28	51	21	0.55
0.6	1.2	0.8	25	44	31	0.56
0.2	1	1.65	19	34	47	0.56

### 2.2. Characterizations

The structure analysis of the as-deposited and annealed films was carried out by using XRD with a Bruker D8-ADVANCE X-ray diffractometer that used CuK $\alpha$  radiation.

Young's modulus and hardness were measured with a Nano Indenter XP (MTS Systems Corporation, Oak Ridge, TN, USA) with a continuous stiffness measurement (CSM) option. A three-sided pyramidal diamond tip (Berkovich indenter) was used, and twenty indents were performed for each sample; their average was considered. The penetration depth was kept as low as possible (less than 10% of the film thickness) so that the influence of the substrate stiffness remained negligible [29].

The thermal behavior of the TFMGs was investigated with an SETSYS Evolution differential scanning calorimetry from SETARAM. Substrate-free films (mass = 0.4 mg) were obtained by depositing TFMGs onto molybdenum foils, the bending of which facilitated their delamination. The DSC chamber was pumped down to a pressure of  $2 \times 10^{-2}$  mbar and then filled up with argon. The measurements were carried out at the same heating and cooling rate (20 °C/min) and from 25 to 700 °C.

In order to investigate thermal stability, the TFMGs were annealed at different temperatures using a vacuum oven (300, 350, 400, 450, and 500 °C). The heating rate was 20 °C/min.

Elemental composition and morphology were investigated with energy dispersive X-ray spectroscopy (EDX) by means of a Hitachi SU8030 scanning electron microscope (Hitachi High-Technologies Corporation, Tokyo, Japan).

### 3. Results and Discussion

#### 3.1. Elemental Composition and Morphology

The discharge currents and the corresponding elemental compositions of the Cu-Zr(-Ta) films are summarized in Table 1. It is clearly shown that the Cu at %/Zr at % ratio remained quite constant, while the tantalum content increased from 0 to 47 at %. Figure 1 shows the cross-sectional SEM images of two different compositions (without Ta and with 31 at % Ta). All the films had the same glassy morphology: viscous-like features with shear striations and partial vein patterns, implying the typical rupture characteristic of the BMGs [30].

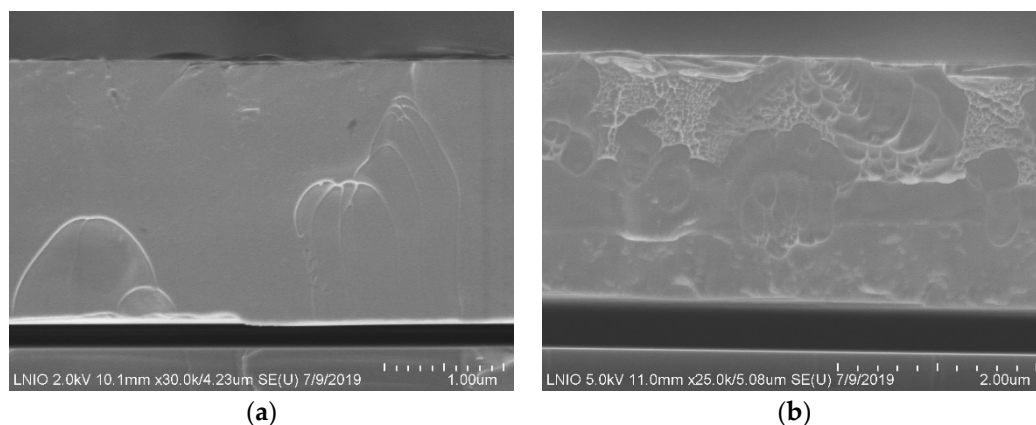
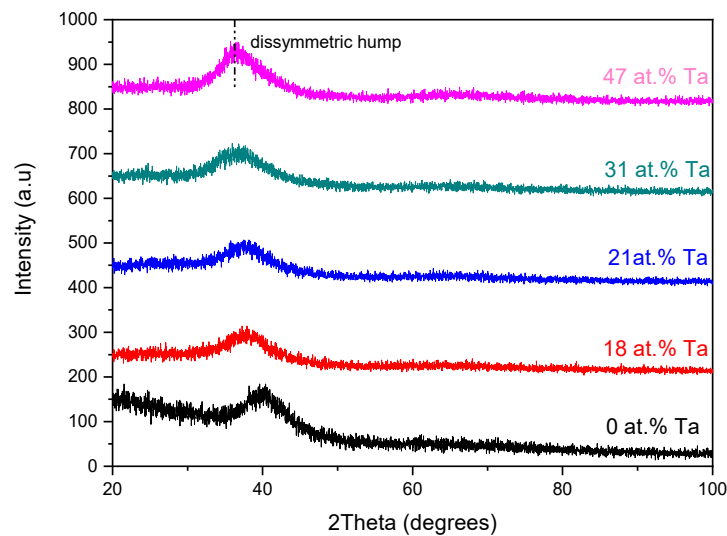


**Figure 1.** The cross-sectional SEM images of deposited thin film metallic glasses (TFMGs): (a) 0 at % of Ta; (b) 30 at % of Ta.

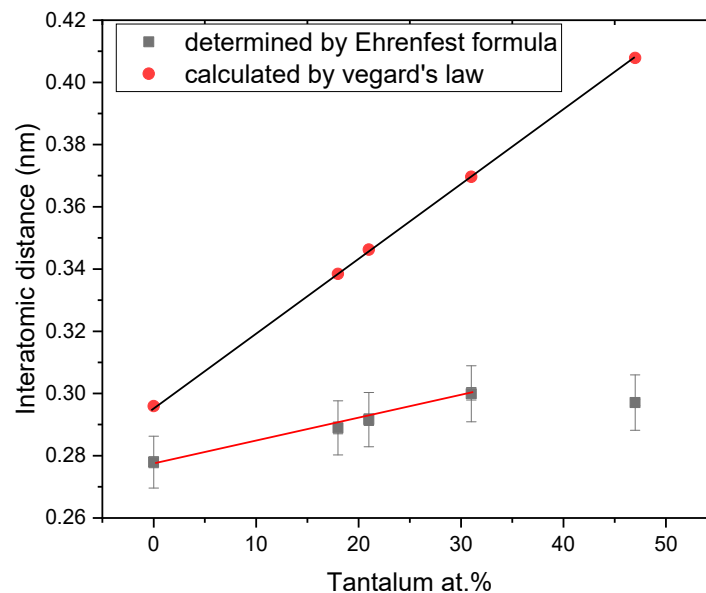
#### 3.2. Structure

Figure 2 shows the XRD  $\theta$ - $2\theta$  patterns of the as-deposited Cu-Zr(-Ta) films as a function of Ta content. A diffuse broad hump at  $2\theta$  diffraction angles ranging between  $35^\circ$  and  $45^\circ$ , as characteristic of amorphous materials, was observed for all diffractograms. This could mean that some crystalline nanodomains were present in the amorphous matrix. However, due to X-ray detection limitations, they were not detected. Figure 3 shows the evolution, as a function of Ta content, of the mean distance between the first neighbors determined from Figure 2 with the Ehrenfest formula [31] and calculated from Vegard's law. Despite the atom radius of each element ( $r(\text{Ta}) = 0.147$  nm,  $r(\text{Cu}) = 0.145$  nm, and  $r(\text{Zr}) = 0.206$  nm), the mean distance between the first neighbors increased with Ta content up to 31 at % Ta. Additionally, the experimental values were much lower the calculated values, which highlighted the dense atomic packing state of the films. The diffuse hump of the Cu-Zr(-Ta) film with 47 at % Ta was clearly dissymmetric (Figure 2), which could have been due to precipitation of a Ta-based nanocrystalline phase. This precipitation could have led to a loss in Ta in the amorphous matrix associated with a slight decrease of the mean distance between the first neighbors of the amorphous phase.

A similar dependence was observed for the Cu-Ta TFMG when the Ta content was increased [32]. This was essentially related to the volume expansion that was induced by the strong repulsive interaction in the atomic potential [33].



**Figure 2.** XRD diffractograms of as-deposited films as a function of Ta content. Dash line for the diffractogram of the film with 47 at % Ta highlights the dissymmetry of the hump.



**Figure 3.** Evolution as a function of the tantalum content of the mean distance between the first neighbors determined by Ehrenfest formula and calculated by Vegard's law.

### 3.3. Mechanical Properties

The nanoindentation charge–discharge curves of the deposited TFMGs are presented Figure 4. The plastic deformation ratio was calculated from nanoindentation curves according to Equation (1):

$$\text{Plastic deformation ratio} = (\text{permanent deformation})/(\text{total deformation}) \quad (1)$$

Figure 5 shows the evolution of this ratio as a function of the tantalum content. It is clear that this ratio remained constant at about 0.73 when the tantalum content was below 21 at %. However, this ratio decreased to 0.63 and 0.62 for 31 at % and 47 at % Ta, respectively. This means that the ductility of the deposited TFMGs decreased significantly at higher tantalum contents, e.g., 31 at % and 47 at %.

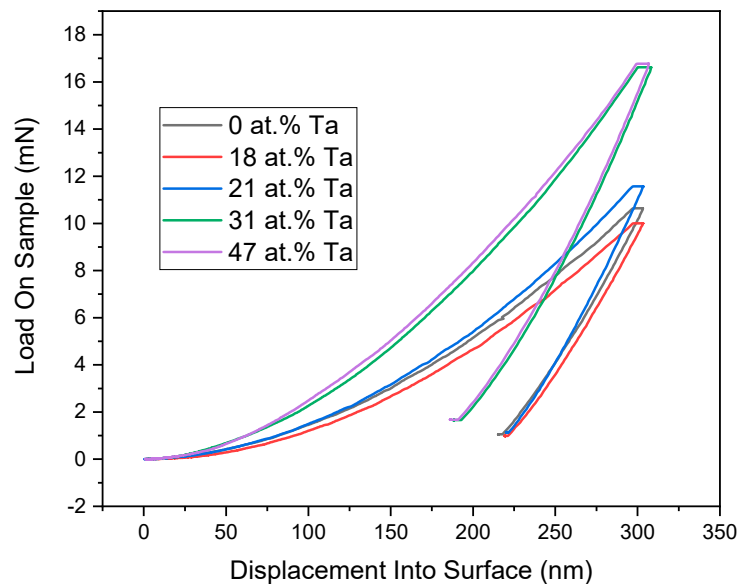


Figure 4. Nanoindentation curves of deposited films.

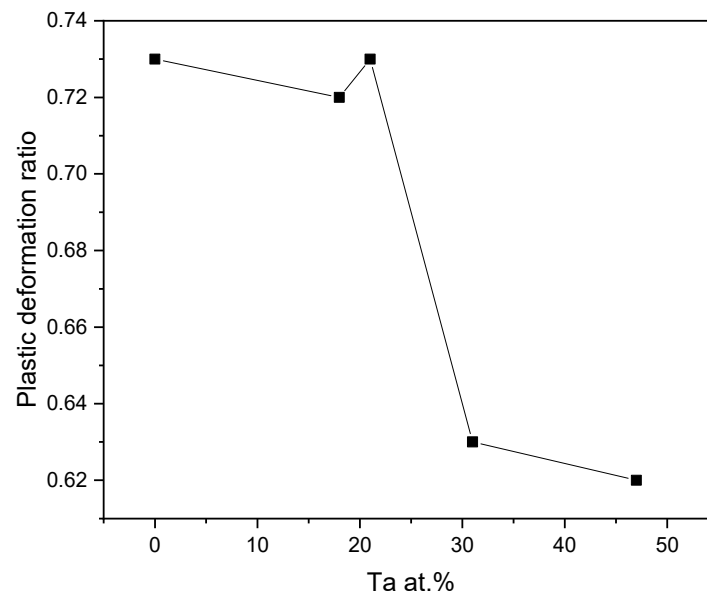
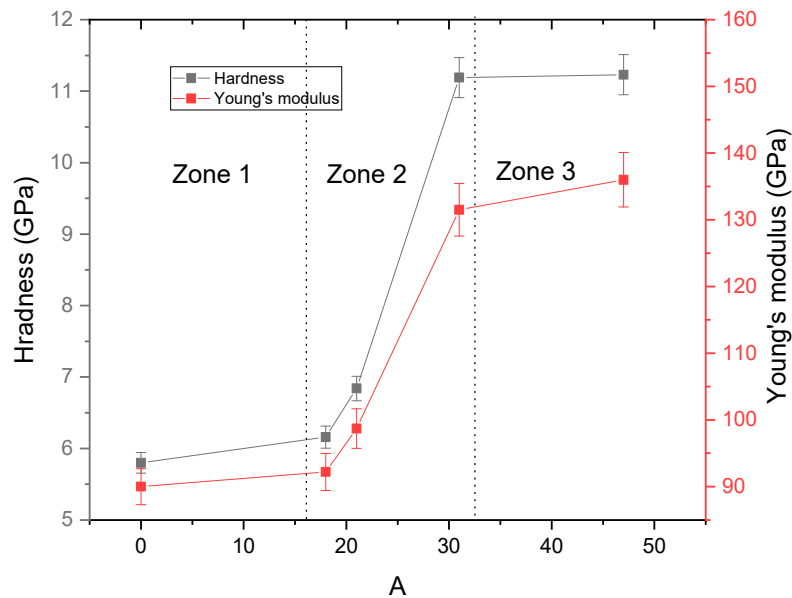


Figure 5. Evolution of plastic deformation ratio as a function of tantalum content.

Figure 6 clearly shows that the tantalum addition led to a significant increase of the hardness and Young's modulus of the as-deposited TFMGs from 5.8 to 11.23 Gpa and from 90 to 136 Gpa, respectively. Chou et al. [25] and Zneg et al. [32] observed the same behavior when tantalum was added to Zr-Cu-Ti and Cu-Ta TFMGs, respectively. The highest hardness of the binary Cu-Zr amorphous single phased films was measured at 6.5 GPa [10]. This mechanism is essentially based on the amorphous material density, which is linked to the cohesion energy of the material. The substitution of copper and zirconium by tantalum promoted the atomic packing state of the films; the difference between the experimental and calculated values of the mean distance between the first neighbors increased with Ta content (Section 3.2, Figure 3), which promoted a higher hardness and a higher Young's modulus. Figure 6 shows a threshold above which the rise of both hardness and Young's modulus was sharp (Zone 2; Figure 6). Regarding the fact that the mean distance between the first neighbors increased with Ta content, the increase of hardness and Young's modulus up to 31 at % Ta could be mainly explained by a higher bond energy due to the more covalent character of the metallic-covalent bonds of Ta (Ta exhibits a larger overlap of the d-orbitals than Zr and Cu). The hardness stabilization at

47 at % Ta (Zone 3, Figure 6) could have been due to the precipitation of a Ta-based crystalline phase, as discussed in Section 3.2, that was slightly detected by the XRD (Figure 2) and that led to a loss in Ta of the amorphous matrix. A similar effect has been revealed for a Cu-Hf-Ti-Ag-Ta BMG/dendrite composite [34]. The hardness of this composite decreased from 9.66 to 9.36 GPa when the volume fraction of the dendritic phase increased from 4.3 to 26.5 vol%.



**Figure 6.** Evolution of Young's modulus and hardness as a function of tantalum content.

The Young's modulus could be determined by the following equation [30]:

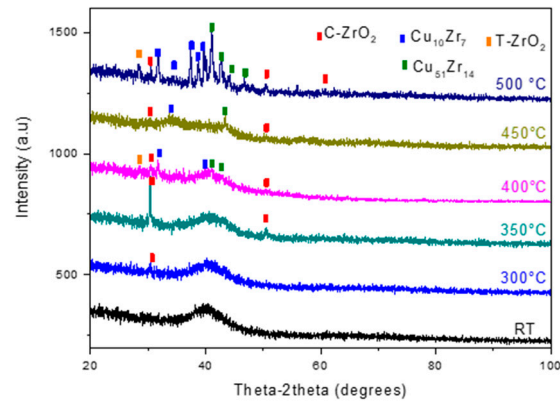
$$E = Kr \frac{\partial}{\partial r} \left( \frac{1}{r^2} \frac{\partial U}{\partial r} \right) \quad (2)$$

where  $E$  is the elastic modulus,  $U$  is the interatomic potential,  $r$  is the interatomic distance, and  $k$  is a constant. According to this equation, the Young's modulus could be influenced by two parameters: the interatomic distance and the interatomic potential. The evolution of  $E$  can also be explained by the competition between inter-atomic distance and the strong variation of the potential gradient [32]. It is well known that a strong repulsive interaction exists in inter-atomic potential after amorphization [33]. Indeed, the incorporation of one element with a different atomic size into the matrix of another element leads to the appearance of a strong repulsive interaction without a change of the attractive interaction [32]. This strong repulsive interaction leads to a sharp variation of the potential gradient around the equilibrium inter-atomic distance by very strongly compressing the well of the inter-atomic potential [32]. If the effect of the potential gradient variation overcomes that of the inter-atomic distance enlargement, the Young's modulus increases.

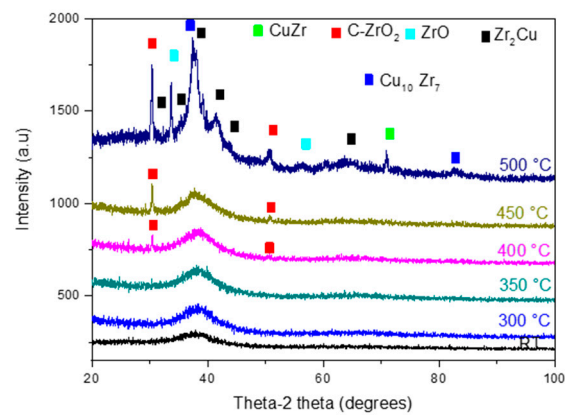
#### 3.4. Thermal Stability

The Cu-Zr(-Ta) films were annealed at different temperatures (300, 350, 400, 450, and 500 °C) over two hours under vacuum ( $10^{-2}$  Pa). Figure 7 shows the structural evolution as a function of annealing temperatures. Tetragonal  $ZrO_2$  was observed above 300 °C for films without Ta (Figure 7a). It could also be observed that the heating of this film at higher temperatures led to the crystallization of  $Cu_{10}Zr_7$  at 400 °C. Other crystalline phases were detected at higher heating temperatures, e.g.,  $Cu_{51}Zr_{14}$ . This behavior, without Ta, was consistent with other studies on the thermal stability of binary Cu-Zr TFMGs [10,11]. Despite vacuum conditions during annealing, the high reactivity of zirconium for oxygen is so high that zirconia grows [35]. Figure 7b shows the structural evolution of

Cu-Zr-Ta containing 18 at % of tantalum. This film, which showed an enhanced thermal stability, had a delayed oxidation temperature with the crystallization of  $ZrO_2$  from 400 °C. The amorphous phase was entirely transformed at 500 °C. The Cu-Zr-Ta film containing 21 at % of tantalum (Figure 7c) showed a higher thermal behavior, with the crystallization of zirconia starting at 450 °C. For the highest Ta contents, 31 at % (Figure 7d) and 47 at % (Figure 7e), the structure remained stable until 500 °C.

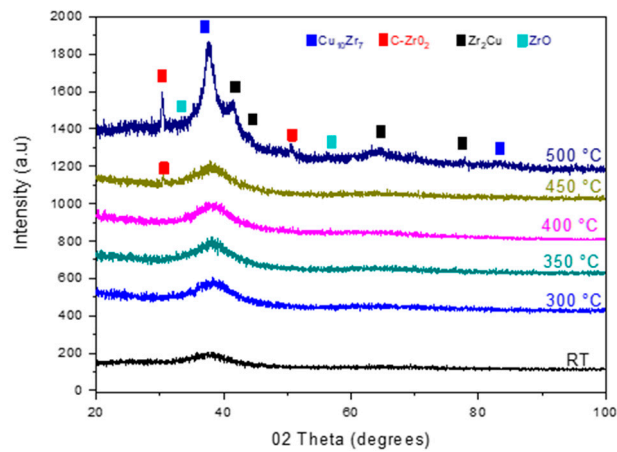


(a)

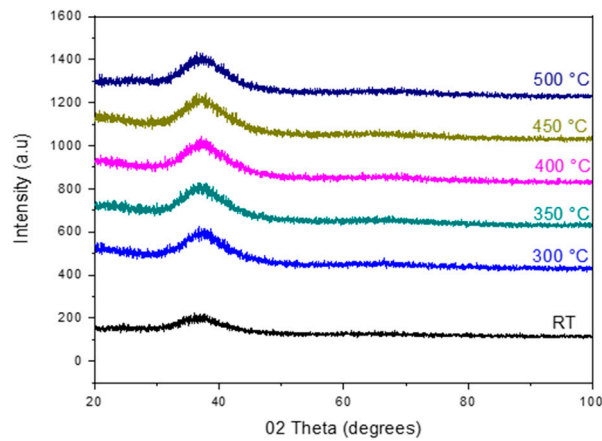


(b)

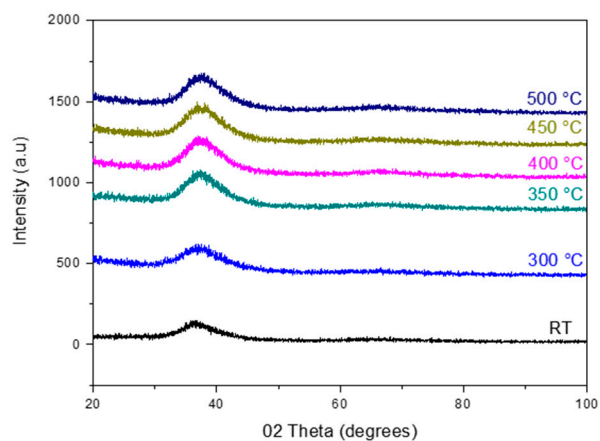
Figure 7. Cont.



(c)



(d)



(e)

**Figure 7.** XRD patterns of Ta-free TFGM, (a) without Ta, (b) 18 at % Ta, (c) 21 at % of Ta, (d) 31 at % of Ta, and (e) 47 at % of Ta, annealed at different temperatures.

The Cu-Zr(-Ta) films were annealed under argon up to 700 °C using a differential scanning calorimeter. The DSC curve of the Ta-free TFGM, presented in Figure 8, shows an exothermic peak at 441 °C, which is preceded by a decrease of the heat flow. This well-known phenomenon [7] is a characteristic of metallic glasses.

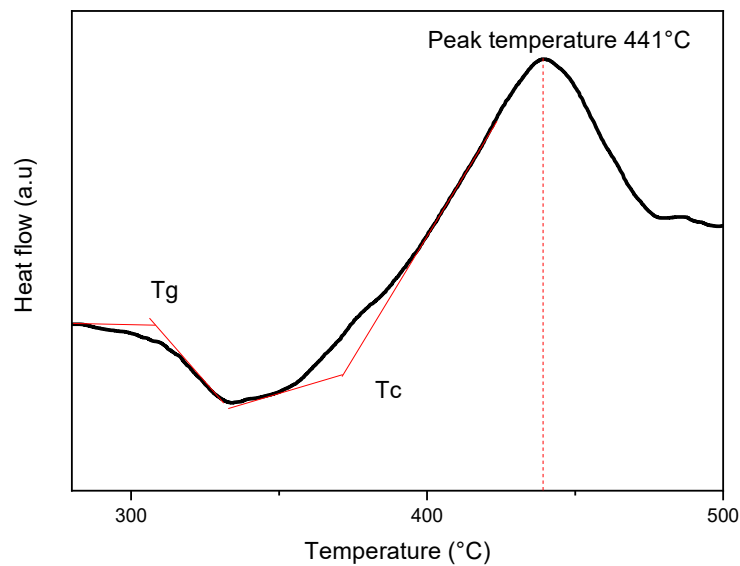


**Figure 8.** DSC curve of the Ta-free TFMG containing 36 at % of Cu and 64 at % of Zr. T<sub>g</sub>: glass transition temperature; T<sub>c</sub>: crystallization temperature.

Table 2 summarizes the values of the glass transition temperature (T<sub>g</sub>) and crystallization temperature (T<sub>c</sub>) determined from DSC curves. It is clearly seen that the crystallization temperature increased with increasing tantalum content between 0 and 31 at %. Then, these temperatures stabilized (for 47 at % Ta). This may be explained, here again, by a higher bond energy due to the more covalent character of the metallic–covalent bonds of Ta, as well as by a lower mobility of Ta during heat treatment. Concerning the slight crystallization temperature decrease for the 47 at % Ta TFMG, the same behavior was observed by Zeman et al. for a Cu–Zr TFMG [15]. This decrease could be attributed to the increase of the nanocrystal fraction, considered nucleation sites that facilitate the crystallization at low temperatures. Indeed, as discussed in Sections 3.2 and 3.3, the dissymmetry of the diffuse hump of the XRD pattern for 47 at % Ta showed that a crystalline phase was present in the amorphous matrix (Figure 2).

**Table 2.** Crystallization and glass transition temperatures as a function of Ta content.

Ta Content (at %)	0	18	21	31	47
T <sub>g</sub> (°C)	308	437	472	520	516
T <sub>c</sub> (°C)	377	462	501	582	577

#### 4. Conclusions

Cu–Zr(–Ta) films were deposited through the DC magnetron sputtering of pure metallic targets in a dynamic mode. The effects of the tantalum addition on the microstructure, mechanical properties, and thermal behavior of the Cu–Zr(–Ta) TFMGs were investigated. The following conclusions can be drawn.

The control of the discharge currents allowed for the addition of Ta without changing the Cu at %/Zr at % ratio. The microstructure showed dependence to tantalum content. It was found that, despite the atom radius of each element, the mean distance between the first neighbors increased with Ta content. Experimental values were much lower than the calculated values, which highlights the dense atomic packing state of the films.

A nanocrystalline phase was slightly detected for 47 at % Ta, and this was associated with a slight decrease of the mean distance between the first neighbors of the amorphous phase.

The substitution of copper and zirconium by tantalum led to an enhancement of the mechanical properties of the Cu–Zr-based TFMG. The hardness and Young’s modulus increased from 5.8 to

11.23 Gpa and from 90 to 136 Gpa, respectively. These results can be attributed to the higher energy of Ta–Ta bonds associated with the covalent character of the metallic–covalent bonds of Ta. The decrease of hardness for 47 at % Ta could have been due to the precipitation of a Ta-based nanocrystalline phase.

It was also found that the thermal behavior of the TFMG was enhanced with tantalum addition. The TFMGs containing 31 and 47 at % showed a good thermal stability (more than 500 °C). The stabilization of T<sub>g</sub> and T<sub>c</sub> for 47 at % Ta can be attributed to nanoprecipitates, which are considered nucleation sites that facilitate crystallization at lower temperatures.

Further investigations with XPS and TEM are planned to validate these hypotheses related to microstructure. Additionally, these films, with an optimized composition, can be potentially used for structural and functional applications, in particular for small-scale applications such as nano- and micro-electromechanical systems (NEMS and MEMS).

**Author Contributions:** Conceptualization, S.A. and F.S.; Methodology, S.A. and F.S.; Validation, F.S.; Formal Analysis, S.A. and F.S.; Investigation, S.A.; Data Curation, S.A.; Writing—Original Draft Preparation, S.A. and F.S.; Writing—Review & Editing, S.A. and F.S.; Supervision, F.S.; Project Administration, S.A. and F.S.; Funding Acquisition, F.S. All authors have read and agreed to the published version of the manuscript.

**Funding:** This research was funded GIP 52 (Groupement d'Intérêt Public) Haute-Marne (annual funding).

**Acknowledgments:** The authors would like to thank GIP5 and Accompagnement Economique du Laboratoire de Bure-Saudron for financial support.

**Conflicts of Interest:** The authors declare no conflict of interest.

## References

1. Telford, M. The case for bulk metallic glass. *Mater. Today* **2004**, *7*, 36–43. [[CrossRef](#)]
2. Ashby, M.F.; Greer, A.L. Metallic glasses as structural materials. *Scr. Mater.* **2006**, *54*, 321–326. [[CrossRef](#)]
3. Greer, A.L. Metallic glasses on the threshold. *Mater. Today* **2009**, *12*, 14–22. [[CrossRef](#)]
4. Schroers, J.; Kumar, G.; Hodges, T.M.; Chan, S.; Kyriakides, T.R. Bulk metallic glasses for biomedical applications. *Jom* **2009**, *61*, 21–29. [[CrossRef](#)]
5. Chu, J.P.; Jang, J.S.C.; Huang, J.C.; Chou, H.S.; Yang, Y.; Ye, J.C.; Wang, Y.C.; Lee, J.W.; Liu, F.X.; Liaw, P.K.; et al. Thin film metallic glasses: Unique properties and potential applications. *Thin Solid Films* **2012**, *520*, 5097–5122. [[CrossRef](#)]
6. Chen, D.Z.; Shi, C.Y.; An, Q.; Zeng, Q.; Mao, W.L.; Goddard, W.A.; Greer, J.R. Fractal atomic-level percolation in metallic glasses. *Science* **2015**, *349*, 1306–1310. [[CrossRef](#)]
7. Zitek, M.; Zeman, P.; Kotrlová, M.; Čerstvý, R.J. Impact of Al or Si addition on properties and oxidation resistance of magnetron sputtered Zr–Hf–Al/Si–Cu metallic glasses. *Alloys Compd.* **2019**, *772*, 409–417. [[CrossRef](#)]
8. Chu, J.; Liu, C.; Mahalingam, T.; Wang, S.; O'Keefe, M.; Johnson, B.C. Annealing-induced full amorphization in a multicomponent metallic film. *Phys. Rev. B* **2004**, *69*, 113410. [[CrossRef](#)]
9. Chiang, P.-T.; Chen, G.-J.; Jian, S.-R.; Shih, Y.-H.; Jang, J.S.-C.; Lai, C.-H.; Fooyin, J. Surface antimicrobial effects of Zr<sub>61</sub>Al<sub>17</sub>.<sub>5</sub>Ni<sub>10</sub>Cu<sub>17</sub>.<sub>5</sub>Si<sub>4</sub> thin film metallic glasses on Escherichia coli, Staphylococcus aureus, Pseudomonas aeruginosa. *Health. Sci.* **2010**, *2*, 12–20.
10. Coddet, P.; Sanchette, F.; Rousset, J.C.; Rapaud, O.; Coddet, C. On the elastic modulus and hardness of co-sputtered Zr–Cu–(N) thin metal glass films. *Surf. Coat. Technol.* **2012**, *206*, 3567–3571. [[CrossRef](#)]
11. Apreutesei, M.; Steyer, P.; Joly-Pottuz, L.; Billard, A.; Qiao, J.; Cardinal, S.; Sanchette, F.; Pelletier, J.M.; Esnouf, C. Microstructural, thermal and mechanical behavior of co-sputtered binary Zr–Cu thin film metallic glasses. *Thin Solid Films* **2014**, *561*, 53–59. [[CrossRef](#)]
12. Apreutesei, M.; Esnouf, C.; Billard, A.; Steyer, P. Impact of local nanocrystallization on mechanical properties in the Zr-59 at % Cu metallic glass thin film. *Mater. Design* **2016**, *108*, 8–12. [[CrossRef](#)]
13. Deng, Y.-L.; Lee, J.-W.; Lou, B.-S.; Duh, J.-G.; Chu, J.P.; Jang, J.S.-C. The fabrication and property evaluation of Zr–Ti–B–Si thin film metallic glass materials. *Surf. Coat. Technol.* **2014**, *259*, 115–122. [[CrossRef](#)]
14. Wang, P.C.; Lee, J.W.; Yang, Y.C.; Lou, B.S. Effects of silicon contents on the characteristics of Zr–Ti–Si–W thin film metallic glasses. *Thin Solid Films* **2016**, *618*, 28–35. [[CrossRef](#)]

15. Zeman, P.; Zítek, M.; Zuzjaková, Š.; Čerstvý, R.J. Amorphous Zr-Cu thin-film alloys with metallic glass behavior. *Alloys Compd.* **2017**, *696*, 1298–1306. [[CrossRef](#)]
16. Bahrami, A.; Carrasco, C.F.O.; Cardona, A.D.; Huminiuc, T.; Polcar, T.; Rodil, S.E. Mechanical properties and microstructural stability of CuTa/Cu composite coatings. *Surf. Coat. Technol.* **2019**, *364*, 22–31. [[CrossRef](#)]
17. Jia, P.; Huang, R.; Zhang, S.; Wang, E.; Yao, J.J. Synthesis of Ag-Cr thin film metallic glasses with enhanced sulfide-resistance. *Mater. Technol.* **2020**, *53*, 32–36. [[CrossRef](#)]
18. Zhang, B.; Jia, Y.; Wang, S.; Li, G.; Shan, S.; Zhan, Z.; Liu, R.; Wang, W.J. Effect of silicon addition on the glass-forming ability of a Zr-Cu-based alloy. *Alloys Compd.* **2009**, *468*, 187–190. [[CrossRef](#)]
19. Choi-Yim, H.; Busch, R.; Johnson, W.L. The effect of silicon on the glass forming ability of the bulk metallic glass forming alloy during processing of composites. *J. Appl. Phys.* **1998**, *83*, 7993–7997. [[CrossRef](#)]
20. Hata, S.; Sato, K.; Shimokohbe, A. Fabrication of thin film metallic glass and its application to microactuators. *Proc. SPIE* **1999**, *97*, 3892.
21. Sharma, P.; Zhang, W.; Amiya, K.; Kimura, H.; Inoue, A. Nanoscale patterning of Zr-Al-Cu-Ni metallic glass thin films deposited by magnetron sputtering. *J. Nanosci. Nanotechnol.* **2005**, *5*, 416–420. [[CrossRef](#)]
22. Bouala, G.N.; Etiemble, A.; Der Loughian, C.; Langlois, C.; Pierson, J.F.; Steyer, P. Silver influence on the antibacterial activity of multi-functional Zr-Cu based thin film metallic glasses. *Surf. Coat. Technol.* **2018**, *343*, 108–114. [[CrossRef](#)]
23. Zong, H.; Geng, C.; Kang, C.; Cao, G.; Li, L.; Zhang, B.; Li, M. Excellent near-infrared transmission of Zr-based thin film metallic glasses. *Results Phys.* **2018**, *10*, 612–615. [[CrossRef](#)]
24. Chen, P.-S.; Chen, H.-W.; Duh, J.-G.; Lee, J.-W.; Shian, J.; Jang, C. Characterization of mechanical properties and adhesion of Ta-Zr-Cu-Al-Ag thin film metallic glasses. *Surf. Coat. Technol.* **2013**, *231*, 332–336. [[CrossRef](#)]
25. Chou, H.S.; Huang, J.C.; Chang, L.W. Mechanical properties of ZrCuTi thin film metallic glass with high content of immiscible tantalum. *Surf. Coat. Technol.* **2010**, *205*, 587. [[CrossRef](#)]
26. Pierson, H.O. *Handbook of Refractory Carbides & Nitrides: Properties, Characteristics, Processing and Apps*; William Andrew: Noyes, NJ, USA, 1996.
27. Gatterer, J.; Dufek, G.; Etmayer, P.; Kieffer, R. Monatsh. The cubic tantalum mononitride (B 1) and its mixability with the isotypic mononitrides and monocarbides of the 4a and 5a group metals. *Mon. für Chem.* **1975**, *106*, 1137–1147. [[CrossRef](#)]
28. Meng, D.; Yi, D.J.; Zhao, Q.; Ding, D.W.; Bai, H.Y.; Pan, M.X.; Wang, W.H.J. Tantalum based bulk metallic glasses. *J. Non-Cryst. Solids* **2011**, *357*, 1787–1790. [[CrossRef](#)]
29. Westbrook, J.H. *Splat Cooling and Metastable Phases*; American Society for Metals: Metals Park, OH, USA, 1973.
30. Dal, F.H.; Dubach, J.S.; Löffler, J.F. Shear striations and deformation kinetics in highly deformed Zr-based bulk metallic glasses. *Acta Mater.* **2008**, *56*, 4635.
31. Rachek, O.P. X-ray diffraction study of amorphous alloys Al-Ni-Ce-Sc with using Ehrenfest's formula. *J. Non-Cryst. Solids* **2006**, *352*, 3781–3786. [[CrossRef](#)]
32. Zeng, F.; Gao, Y.; Li, L.; Li, D.M.; Pan, F. Elastic modulus and hardness of Cu-Ta amorphous films. *J. Alloys Compd.* **2005**, *389*, 75–79. [[CrossRef](#)]
33. Gong, H.R.; Kong, L.T.; Lai, W.S.; Liu, B.X. Atomistic modeling of solid-state amorphization in an immiscible Cu-Ta system. *Phys. Rev. B* **2002**, *66*, 104204. [[CrossRef](#)]
34. Bian, Z.; Kato, H.; Qin, C.L.; Zhang, W.; Inoue, A. Cu-Hf-Ti-Ag-Ta bulk metallic glass composites and their properties. *Acta Mater.* **2005**, *53*, 2037. [[CrossRef](#)]
35. Apreutesei, M.; Steyer, P.; Billard, A.; Joly-Pottuz, L.; Esnouf, C.J. Zr-Cu thin film metallic glasses: An assessment of the thermal stability and phases' transformation mechanisms. *Alloys Compd.* **2015**, *619*, 284–292. [[CrossRef](#)]

